



CHORUS

This is the accepted manuscript made available via CHORUS. The article has been published as:

Search for the Neutron Decay $n \rightarrow X + \gamma$, Where X is a Dark Matter Particle

Z. Tang, M. Blatnik, L. J. Broussard, J. H. Choi, S. M. Clayton, C. Cude-Woods, S. Currie, D. E. Fellers, E. M. Fries, P. Geltenbort, F. Gonzalez, K. P. Hickerson, T. M. Ito, C.-Y. Liu, S. W. T. MacDonald, M. Makela, C. L. Morris, C. M. O'Shaughnessy, R. W. Pattie, Jr., B. Plaster, D. J. Salvat, A. Saunders, Z. Wang, A. R. Young, and B. A. Zeck

Phys. Rev. Lett. **121**, 022505 — Published 11 July 2018

DOI: [10.1103/PhysRevLett.121.022505](https://doi.org/10.1103/PhysRevLett.121.022505)

Search for the Neutron Decay $n \rightarrow X + \gamma$, where X is a dark matter particle.

Z. Tang¹, M. Blatnik², L. J. Broussard³, J. H. Choi⁴, S. M. Clayton¹, C. Cude-Woods^{1,4}, S. Currie¹, D. E. Fellers¹, E. M. Fries², P. Geltenbort⁵, F. Gonzalez⁶, K. P. Hickerson², T. M. Ito¹, C.-Y. Liu⁶, S. W. T. MacDonald¹, M. Makela¹, C. L. Morris¹, C. M. O'Shaughnessy¹, R. W. Pattie Jr.¹, B. Plaster⁷, D. J. Salvat⁸, A. Saunders¹, Z. Wang¹, A. R. Young^{1,4}, and B. A. Zeck^{1,4}

¹*Los Alamos National Laboratory, Los Alamos, New Mexico 87545, USA*

²*Kellogg Radiation Laboratory, California Institute of Technology, Pasadena, CA 91125, USA*

³*Oak Ridge National Laboratory, Oak Ridge, Tennessee 37831, USA*

⁴*North Carolina State University, Raleigh, North Carolina 27695, USA*

⁵*Institut Laue-Langevin, Grenoble, France*

⁶*Department of Physics, Indiana University, Bloomington, Indiana 47408, USA*

⁷*University of Kentucky, Lexington, Kentucky 40506, USA*

⁸*University of Washington, Seattle, WA 98195-1560, USA*

Abstract. Fornal and Grinstein recently proposed that the discrepancy between two different methods of neutron lifetime measurements, the beam and bottle methods can be explained by a previously unobserved dark matter decay mode, $n \rightarrow X + \gamma$. We have performed a search for this decay mode over the allowed range of energies of the monoenergetic gamma ray for X to be a dark matter. A Compton-suppressed high-purity germanium detector was used to identify γ -rays from neutron decay in nickel-phosphorous coated stainless-steel bottle. A combination of Monte Carlo and radioactive source calibrations was used to determine the absolute efficiency for detecting γ -rays arising from the dark matter decay mode. We exclude the possibility of a sufficiently strong branch to explain the lifetime discrepancy with 97% confidence.

Keywords: Ultracold neutrons, Dark Matter, LANL UCN facility, Neutron lifetime.

PACS: 14.2.Dh

There is nearly a five standard-deviation disagreement[1,2] between measurements of the rate of neutron decay producing protons measured in cold neutron beam experiments[3-5] (888.0 ± 2.0 s) and free neutron lifetime in bottle experiments [6-8] (878.1 ± 0.5 s). The cold neutron beam method consists of

counting the number of protons emitted from neutron beta decay in a well-characterized neutron beam, and the bottle experiments measure the number of ultra-cold neutrons (UCN) that remain inside a trap after a certain storage time. A longer lifetime from the beam measurements could point to the existence of possible other decay modes of the neutron where a proton is not produced. Serebrov has suggested the discrepancy could be due to neutrons oscillating into mirror neutrons [9,10]. Recently, Fornal and Grinstein have suggested in Ref. [11] that the neutron lifetime discrepancy can be explained if the neutron decayed into a γ -ray and a dark matter particle, X. The γ -ray has an allowable energy range of 782 to 1664 keV, where it is bounded from above by the stability of ${}^9\text{Be}$ and bounded from below by requiring X to be stable.

Here we report the results of a search for γ -rays arising from UCN decaying inside a nickel phosphorous coated [12], 560 L stainless steel bottle. The bottle is filled with UCN from the Los Alamos UCN facility[13] parasitically during the running of the UCN τ experiment[7], with the source operated in production mode. The γ -rays are detected in a lead shielded, Compton scattering suppressed 140% high purity germanium (HPGe) detector [Figure 1]. The Compton scattering suppression is achieved by an anti-coincidence with an annular bismuth germinate (BGO) detector surrounding the HPGe detector. The Compton suppression reduced the background in the low energy part of the spectrum by a factor of 1.7. A gate valve placed upstream controlled loading of UCN into the bottle. The background γ rates were measured with the UCN in production mode and the gate valve closed. This resulted in a factor of 4 reduction in the continuum background in the region of interest (ROI).

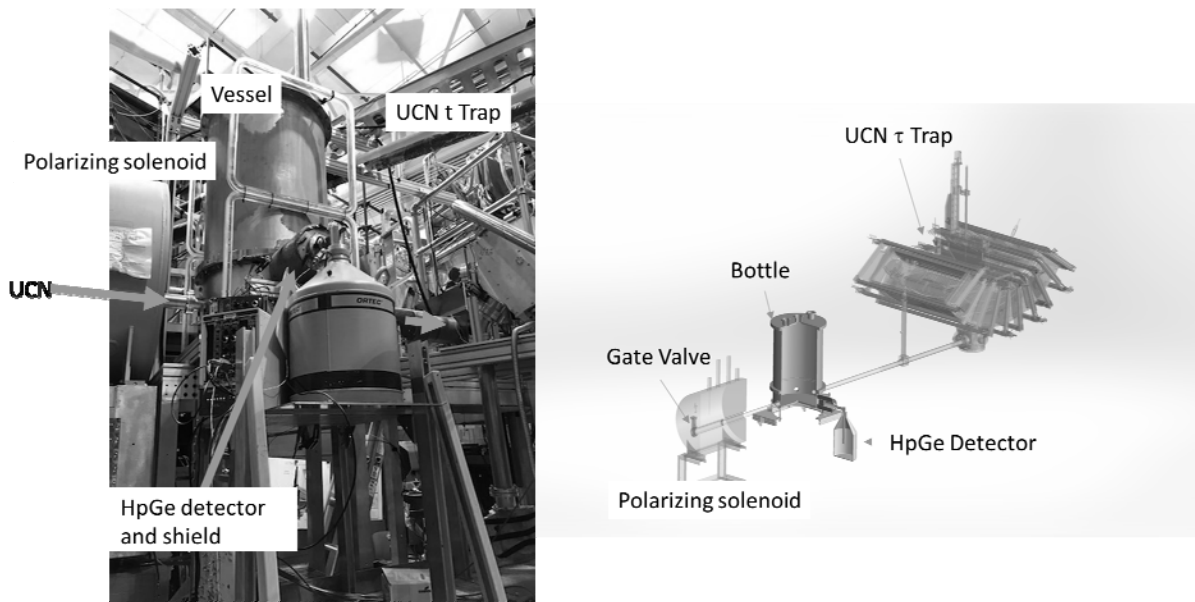


Figure 1: The UCN bottle is installed in the existing beamline, and a HPGe detector is placed next to the outer wall of the vessel. The UCN gate valve is located upstream of the polarizing solenoid magnet. On the left is a photograph of our setup and on the right is a schematic.

The energy calibration of the HPGe spectrum was obtained from a linear fit to 13 gamma ray lines from sources, natural backgrounds and prominent neutron capture lines on ${}^{58}\text{Ni}$, ${}^{56}\text{Fe}$, and ${}^{35}\text{Cl}$. The UCN induced gamma-ray spectrum was then constructed by subtracting the background spectrum (gate valve closed)

from the foreground spectrum (gate valve open). The results of this subtraction are shown in Figure 2. The peaks in the spectrum are dominated by neutron capture lines on the Ni-P surface and in the stainless steel bulk of the storage vessel. The bulk neutron capture is due to UCN upscattering on the surface of the coating and subsequent capture in the vessel wall. We have identified 22 prompt gamma lines from neutron capture on ^{35}Cl , ^{50}Cr , ^{52}Cr , ^{53}Cr , ^{56}Fe , ^{58}Ni , ^{60}Ni , ^{62}Ni , ^{63}Ni , and ^{64}Ni in the ROI. There were also 2 lines present from the beta delayed gamma rays from ^{24}Na , and ^{56}Mn . Nickel is present both in the coating material and in the bulk stainless steel, which also contains iron, chromium, and manganese. Chlorine is used in surface preparation during the nickel phosphorus coating process. Multiple lines outside of the ROI were also identified for chlorine, iron, chromium, and manganese, which helped the isotope identification process. Sodium-24 is produced in the biological shielding stack, and it is present in both the foreground and background measurements. However, due to its long half-life (14.96 hours) and the sequential order of the foreground and background measurements, the background subtraction produced a small negative peak.

The experiment was modeled using GEANT4[14]. The detector efficiency-solid angle product was measured using the 1333 keV gamma line from a calibrated ^{60}Co source. The simulation reproduced the calibration measurements to within 5% for all points on a vertical scan through the UCN bottle with no adjustable parameters, using the known detector configuration and experiment geometry. The absolute predicted and measured efficiency-solid angle product at 1333 keV agreed within 5%. This allowed the strengths of the gamma lines in the allow region to be computed by normalizing to peaks from the same isotope outside of the allowed region using the relative peak strengths given in Ref. [15], after correcting for the energy dependence of the detector efficiency given by the GEANT4 calculation. This procedure accounts for the unknown capture/production rates for each isotope that produces gamma rays in the allowed region experimentally, using only information from outside of the allowed energy region. The normalization had a single global scaling factor and a single factor to normalize all lines from each isotope after correcting for detector efficiency. The results are given in Table 1 and Figure 2.

Table 1) list of origin, strength, and normalization for all of the lines subtracted in the ROI. When two lines are listed in the normalization column, both were used to obtain the normalization and their summed strength is given

| Isotope | Energy KeV | Strength cnts/10 s | Normalization | | Isotope | Energy KeV | Strength cnts/10 s | Normalization | |
|------------------|---------------|--------------------------|---------------|-----------------------|------------------|---------------|--------------------------|---------------|---------------------|
| | | | Energy keV | Strength cnts/10 s | | | | Energy keV | Strength cnts/10 |
| ³⁵ Cl | 788 | 0.108 | 6110+7414 | 0.058 | ⁶⁴ Ni | 1107 | 0.002 | 6034.8 | 0.013 |
| ⁶⁰ Ni | 817 | 0.030 | 7820 | 0.221 | ⁵⁰ Cr | 1149 | 0.022 | 1899 | 0.068 |
| ⁵³ Cr | 835 | 1.254 | 2239 | 0.110 | ³⁵ Cl | 1165 | 0.159 | 6110+7414 | 0.058 |
| ⁶² Ni | 846 | 0.023 | 6838 | 0.327 | ⁶⁰ Ni | 1185 | 0.036 | 7820 | 0.221 |
| ⁵⁶ Mn | 846 | 0.204 | 1810 | 0.040 | ⁵⁸ Ni | 1189 | 0.124 | 8534 | 0.431 |
| ⁵⁸ Ni | 878 | 0.587 | 8534 | 0.431 | ⁵⁶ Fe | 1261 | 0.122 | 7631 | 0.390 |
| ⁵⁰ Cr | 888 | 0.017 | 1899 | 0.068 | ⁵² Cr | 1289 | 0.045 | 7939+7940 | 0.059 |
| ⁵⁶ Fe | 898 | 0.105 | 7631 | 0.390 | ⁵⁸ Ni | 1301 | 0.119 | 8534 | 0.431 |
| ⁶⁰ Ni | 939 | 0.012 | 7820 | 0.221 | ⁶⁴ Ni | 1346 | 0.001 | 6034.8 | 0.013 |
| ⁵² Cr | 1006 | 0.093 | 7939+7940 | 0.059 | ²⁴ Na | 1369 | -0.462 | 2754 | -0.310 |
| ⁵⁶ Fe | 1019 | 0.092 | 7631 | 0.390 | ⁵⁰ Cr | 1537 | 0.012 | 1899 | 0.068 |
| ⁶⁰ Ni | 1100 | 0.019 | 7820 | 0.221 | ⁵⁶ Fe | 1613 | 0.232 | 7631 | 0.390 |

The strength of each peak inside the ROI was calibrated using the peaks from the same isotope outside of the ROI [15]. A list of the lines, origin, and normalization subtracted in the ROI is given in Table 1. A Geant4[16] simulation was used to obtain the energy dependence of the detector. All detector components, including the lead, bgo, and entrance windows, were included in the Geant calculations. This simulation placed a source at the center of the storage volume and included the wall and the detector windows. A peak with a 4.2 keV Gaussian width (the detector resolution) and a normalized peak strength including the relative peak strengths and detector efficiency was generated for each peak inside the ROI and the sum of all the peaks was subtracted to obtain the thin black curve in Figure 2.

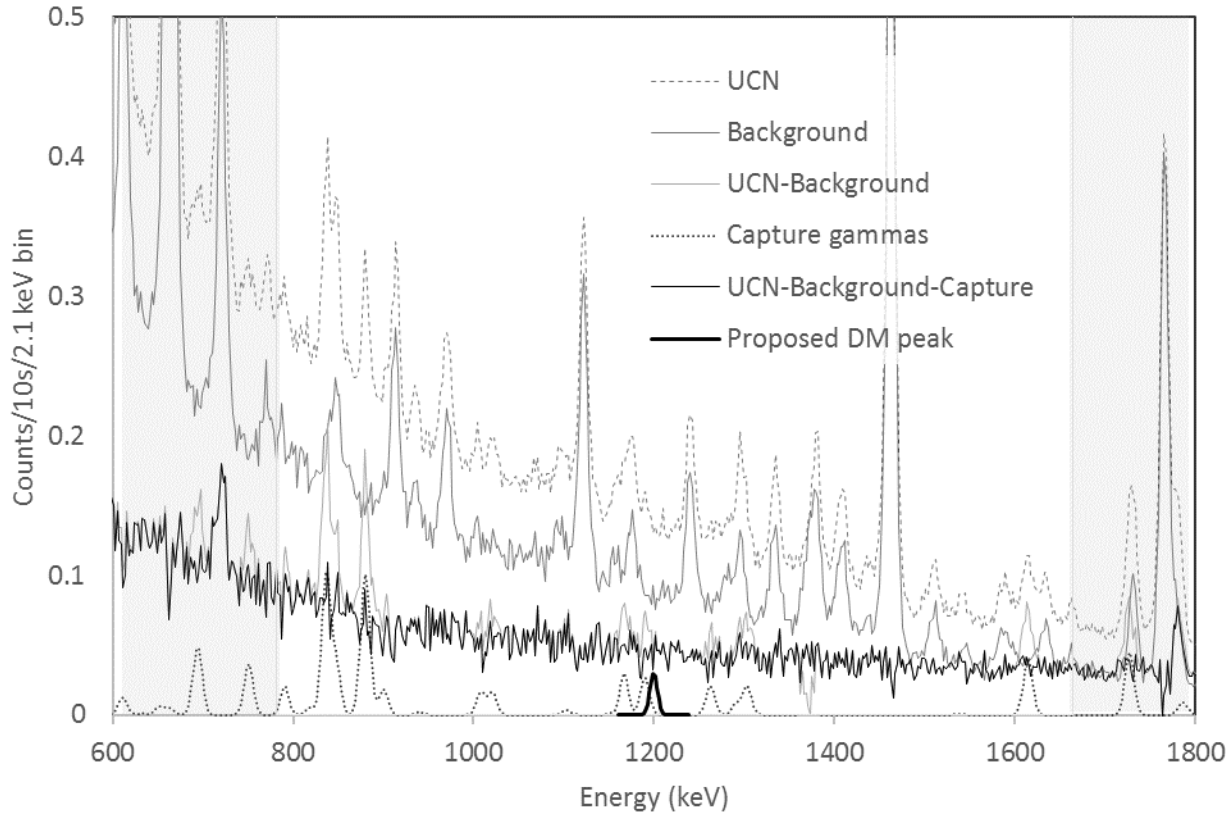


Figure 2: Measured and simulated spectra in the ROI (white background). The blue and red lines show the Compton scattering suppressed spectra for the measurement with UCN and background measurement, respectively. The dotted line shows the simulated spectra from UCN capture and related gamma rays. The grey and thin black curves show the net UCN signal and the net signal after capture gamma subtraction, respectively. The peak plotted with a thick black line centered at 1200 keV shows an example of the size of the proposed decay that would be needed to explain the anomaly.

To determine the rate of decay into this proposed channel, one needs to know the number of UCN inside the storage volume. The UCN density inside this storage volume was measured using the vanadium activation method [17,18]. A 1.0 cm diameter foil was mounted on the inside of the wall of the vessel, near the detector. Due to the negative Fermi potential of the ^{51}V , 84% of UCN that intercept the foil are absorbed and produce ^{52}V , and a correction is made for neutrons that are upscattered or reflected. Neutron capture on ^{51}V produces ^{52}V , which has a beta decay half-life 3.74 minutes, and a 1434 keV γ is produced along with the beta decay 100% of time. This gamma ray is then detected in the HPGe detector. The efficiency of the germanium detector was normalized by using a ^{60}Co source of known activity (9.3 ± 0.9 kBq) that was placed on top of the ^{51}V foil and the rate of 1333 keV γ was measured. This accounted for solid angle and detector efficiency and gamma ray attenuation in the vessel walls. The results were cross calibrated to the measurement by normalizing using upstream $^{10}\text{B}/\text{ZnS}$ UCN monitor detectors [19]. The average UCN density at beam height in the storage volume for the foreground measurement was $\rho_0 = 9.5 \pm 1.3$ UCN/cm³, where the uncertainty is dominated by the corrections to the ^{51}V capture fraction as in ref. [17].

The Ge detector acceptance for γ -rays for each gamma emission position inside the UCN storage vessel was measured by scanning the storage volume with the calibrated ^{60}Co source using the 1333 keV line. The 1333 line was used for normalizations because of the small amount Compton background from lines above it. First, the source was scanned along a line through the center of the detector. This was fitted with the function $a/(z-z_0)^2$, where z was measured from the cylindrical center of the volume. The constants a and z_0 were fitted free parameters. This determined an effective center of the detector relative to the center of the storage vessel. Next, a 2D counting rate scan was made in two axes, the axis of the cylinder (y) and an axis normal to z and y . The experimental acceptance measurements are in good agreement (within 5%) with GEANT4 simulations of our detector geometry. After being normalized to the activity of the source, these data were fitted with a function:

$$R(x, y, z) = \frac{A}{r^2} e^{-\frac{\theta^2}{2\theta_0^2}} \quad (1)$$

where $\theta_0 = \text{atan}\left(\frac{\sqrt{x^2+y^2}}{r}\right)$ and $r = \sqrt{x^2 + y^2 + (z - z_0)^2}$.

The acceptance for gamma rays, A , from neutron decay was obtained by integrating this acceptance over the neutron density, assuming a $dN / dv \propto v^2$ distribution, where v is the neutron velocity and N is the neutron density, and accounting for the gravitational distribution of the density[20]:

$$\begin{aligned} \rho(x, y, z) &= \rho_0 & y < y_{beam} \\ &= \rho_0 \sqrt{\frac{v_{max}^2 - 2gy}{v_{max}^2}} & y_{beam} < y < \frac{v_{max}^2}{2g} \end{aligned} \quad (2)$$

$$A = \int_V R(x, y, z) \rho(x, y, z) dV$$

Where $\rho(x, y, z)$ is the UCN density as a function of position, v_{max} is the maximum UCN velocity, g is the acceleration due to gravity, and the integral is over the volume of the vessel. A $v^2 dv$ velocity distribution up to a maximum velocity of 600 cm/s (given by the Fermi potential of upstream stainless steel guides[20]) is used to determine the height dependence of ρ .

The volume integrated detector sensitivity is 88 ± 9 counts/(decay/cm³). The branching ratio for UCN decay into dark matter needed to explain the difference in the beam and bottle lifetimes is 1.3%, so the decay rate is $1.2 \times 10^{-5} \text{ s}^{-1}$. The measured density gives an expected rate of 11.9 ± 1.2 mHz, or 0.12 counts/10 s for a peak at 1333 keV. The uncertainty is taken to be the uncertainty in the source activity.

In order to estimate the likelihood of a peak with the predicted signal strength, we have fitted a linear background to 100 keV wide segments of the spectrum and integrated the area above the background in a

12 keV wide region (~ 3 Gaussian σ peak widths) centered in the segment, to obtain the peak yield, Y_i . The peak region was excluded from the background fit. This procedure was repeated in 4 keV steps across the spectrum for each bin i . The uncertainties, ΔY_i , were calculated assuming Poisson statistics for the foreground and background spectra. The number of standard deviations (x) between each yield, Y_i , and the predicted signal was calculated as $x_i = \sqrt{(Y_i - P_i)^2 / (\Delta Y_i^2 + \Delta P_i^2)}$, where P_i is the predicted signal and ΔP_i is its uncertainty, obtained by adding the uncertainties in the UCN density and acceptance in quadrature. The likelihood for each i is given by the cumulative normal distribution function. Summing the likelihood over all the 4 keV wide bins in the ROI and dividing by three, to account for the 12 keV wide integration window, accounts for the unknown location of a peak[21] (the so called “look elsewhere effect”) and excludes the presence of a mono-energetic γ ray in the entire ROI with a total confidence limit of 97%. The largest contributor is the fluctuation at 1130 keV, with a probability of 1.6%.

In Figure 3, two peaks at 720 keV and 1779 keV are also shown to demonstrate the sensitivity of our analysis, even though they are outside of the ROI. The 720 keV peak could be due to the decay of ^{10}C , which is a spallation product produced inside the biological shielding stack. The 1779 keV peak is due to the gamma ray generated from the beta decay of ^{28}Al , which was formed by neutron capture on ^{27}Al . The overlap between adjacent bins can be observed in the saturated likelihood for these peaks.

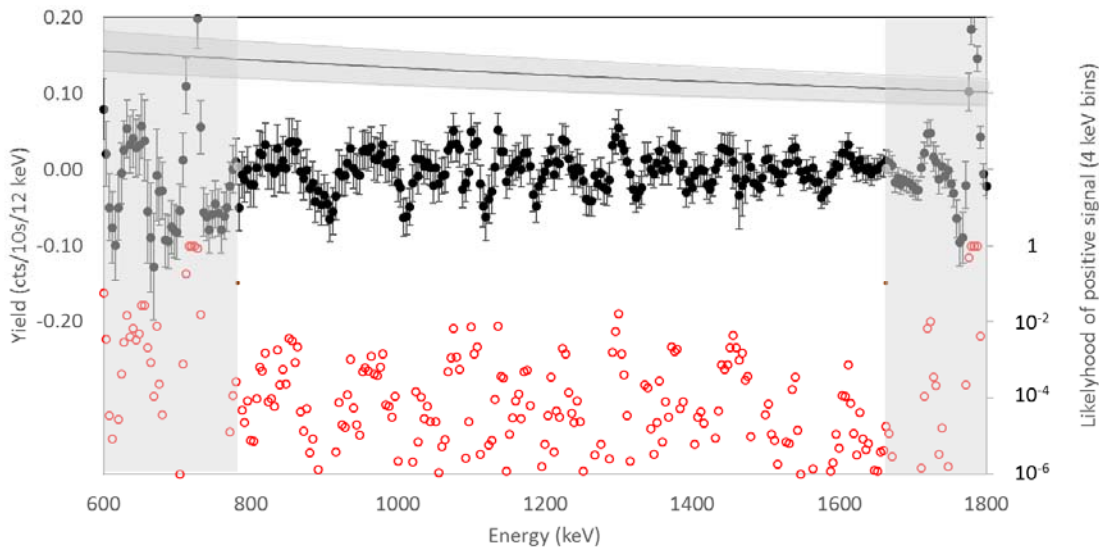


Figure 3 The data (solid circles) plotted are the sum of counts in a 12 keV (~ 3 Gaussian peak widths) window above a piecewise fitted background across the ROI. The integration region is centered in 100 keV wide fitting window, and it is performed in 4 keV steps. The unshaded center of the plot is the ROI. The predicted signal (solid line and shaded region) accounts for the energy dependent photopeak efficiency predicted by GEANT4.[16] The open circles show the likelihood of the predicted signal in each overlapping bin.

In summary, we have used the Los Alamos UCN source[13] to search for monoenergetic gamma rays from neutron decay to dark matter, a solution recently proposed to explain the difference between beam and

bottle neutron lifetime results.[11] Our measurements exclude this possible explanation[11] with 97% confidence.

This work was supported by the Los Alamos Laboratory Directed Research and Development (LDRD) office (No. 20140568DR), the LDRD Program of Oak Ridge National Laboratory, managed by UT-Battelle, LLC (No. 8215), the National Science Foundation (Nos. 130692, 1307426, 161454, 1506459, and 1553861), IU Center for Space Time Symmetries (IUCSS), and DOE Low Energy Nuclear Physics (Nos. DE-FG02-97ER41042, DE-SC0014622, and DE-AC05-00OR22725). The authors would like to thank the staff of LANSCE for their diligent efforts to develop the diagnostics and new techniques required to provide the proton beam for this experiment.

- [1] F. E. Wietfeldt, arXiv preprint arXiv:1411.3687 (2014).
- [2] G. L. Greene and P. Geltenbort, *Scientific American* **314**, 36 (2016).
- [3] J. Byrne *et al.*, *Physical Review Letters*; (USA) **65** (1990).
- [4] A. Yue, M. Dewey, D. Gilliam, G. Greene, A. Laptev, J. Nico, W. Snow, and F. Wietfeldt, *Physical review letters* **111**, 222501 (2013).
- [5] J. Byrne, P. Dawber, C. Habeck, S. Smidt, J. Spain, and A. Williams, *EPL (Europhysics Letters)* **33**, 187 (1996).
- [6] A. Serebrov *et al.*, *Physical Review C* **78**, 035505 (2008).
- [7] C. L. Morris *et al.*, *Review of Scientific Instruments* **88**, 053508 (2017).
- [8] R. Pattie Jr *et al.*, arXiv preprint arXiv:1707.01817 (2017).
- [9] A. Serebrov *et al.*, *Physics Letters B* **663**, 181 (2008).
- [10] Z. Berezhiani and L. Bento, *Physical review letters* **96**, 081801 (2006).
- [11] B. Fornal and B. Grinstein, in *ArXiv e-prints* (2018).
- [12] R. W. Pattie Jr *et al.*, *Nuclear Instruments and Methods in Physics Research Section A: Accelerators, Spectrometers, Detectors and Associated Equipment* **872**, 64 (2017).
- [13] T. M. Ito *et al.*, *Physical Review C* **97**, 012501 (2018).
- [14] S. Agostinelli *et al.*, *Nuclear instruments and methods in physics research section A: Accelerators, Spectrometers, Detectors and Associated Equipment* **506**, 250 (2003).
- [15] Thermal Neutron Capture γ 's (CapGam), <https://www-nds.iaea.org/capgam/index.htmlx> (Accessed February 1 2018).
- [16] J. Allison and e. al., *Nuclear Instruments and Methods in Physics Research A* **836**, 186 (2016).
- [17] A. Saunders *et al.*, *Review of Scientific Instruments* **84**, 013304 (2013).
- [18] A. Frei, K. Schreckenbach, B. Franke, F. Hartmann, T. Huber, R. Picker, S. Paul, and P. Geltenbort, *Nuclear Instruments and Methods in Physics Research Section A: Accelerators, Spectrometers, Detectors and Associated Equipment* **612**, 349 (2010).
- [19] Z. Wang *et al.*, *Nuclear Instruments and Methods in Physics Research Section A: Accelerators, Spectrometers, Detectors and Associated Equipment* **798**, 30 (2015).
- [20] R. Golub, D. Richardson, and S. K. Lamoreaux, *Ultra-cold neutrons* (CRC Press, 1991).
- [21] L. Lyons, *The Annals of Applied Statistics* **2**, 887 (2008).